

High order semi-Lagrangian numerical solutions to the plasma kinetic equation in the edge of magnetic fusion devices

David Sirajuddin, Professor William N.G. Hitchon

University of Wisconsin – Madison
Department of Electrical and Computer Engineering

December 12, 2014



College of Engineering
UNIVERSITY OF WISCONSIN-MADISON



Table of Contents



Overall goal

Aim: To develop high order semi-Lagrangian deterministic solutions to Boltzmann transport equations relevant to plasma dynamics in the edge of magnetic fusion devices. This will include a treatment of collisions as well as accurate modeling of the boundary and associated sheath physics.



Outline



Plasma confinement configurations: tokamaks

Confinement requires toroidal magnetic fields with a poloidal twist

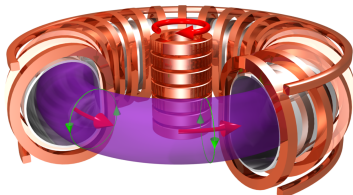


Figure: Typical tokamak configuration

Tokamak configuration

- Toroidal field coils $\Rightarrow B_\phi$
- Plasma current $\Rightarrow B_\theta$
- Poloidal field coils for shaping
- Transformer \Rightarrow pulsed operation

Image: MPI für Plasmaphysik (IPP), accessed from <http://www.ideen2020.de/en/51/energy/>



Core characteristics for two tokamaks

	C-Mod	DIII-D
Parameters		
Major radius R [m]	0.61 – 0.74	1.49 – 1.88
Minor radius a [m]	0.169 – 0.264	0.331 – 0.752
Aspect ratio R/a	2.8 – 3.6	2.5 – 4.5
Magnetic field B [T]	2.0 – 8.0	0.5 – 2.2
Max plasma volume [m^3]	1	24
Max T_i, T_e [keV]	5.6, 6.0	27.0, 16.0
Max current I [MA]	2.05	3
Max power density [MW/m ³]	6.7	1.3
Shot length [s] at B_{\max}	1	6
PFCs	Mo, W	C



Core characteristics for two additional tokamaks

	NSTX	ITER
Parameters		
Major radius R [m]	0.8 – 1.0	6.2
Minor radius a [m]	0.5 – 0.787	2
Aspect ratio R/a	1.27 – 1.6	3.1
Magnetic field B [T]	0.8 ~ 1.6	3.1
Max plasma volume [m^3]	14	700
Max T_i, T_e [keV]	2.5, 4.1	30, 30
Max current I [MA]	1.5	15
Max power density [MW/m ³]	1.1	0.7
Shot length [s] at B_{max}	1.5	400
PFCs	CFC/Graphite Li coating	W, C and Be



Plasma confinement configurations: stellarators

Confinement requires toroidal magnetic fields with a poloidal twist

Stellarator configuration

- modular coils \Rightarrow helical field lines
- no net plasma current required
- steady state operation

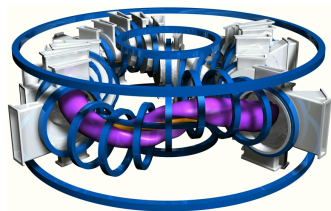


Figure: TJII

Image: Laboratorio Nacional de Fusión, CIEMAT, Madrid.

http://www-fusion.ciemat.es/New_fusion/en/TJII/presentacion.shtml



Core characteristics for two stellarators

	HSX	LHD
Parameters		
Major radius R [m]	1.20 (avg.)	4.0 (avg.)
Minor radius a [m]	0.15 (avg.)	0.6 (avg.)
Aspect ratio R/a	8	6.5
Magnetic field B [T]	1.25	3
No. of field periods/ $2\pi R_0$	4	5
Plasma volume [m^3]	0.44	30
Max T_e [keV]	$\sim 20 - 25$	10
Max power density [MW/m ³]	0.46	0.040
Shot length [s] at B_{max}	1.5	127

Data compiled from <http://www.hsx.wisc.edu/parameters.shtml>,
<http://www.lhd.nifs.ac.jp/en/home/lhd.html>, Fujiwara, M. et al. *Plasma confinement studies in LHD*. IAEA-F1-CN-69/EX2/3, and <http://www.nifs.ac.jp/itc/itc12/Motojima.pdf>



The focus of this work is to simulate the edge

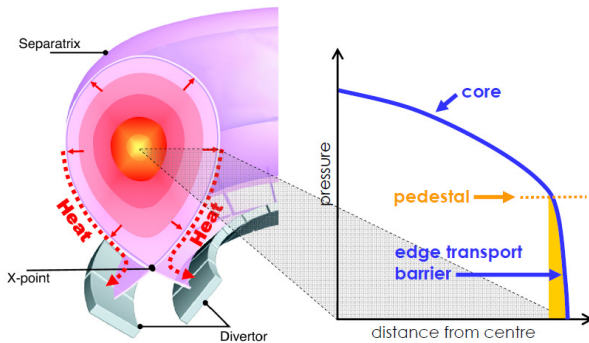
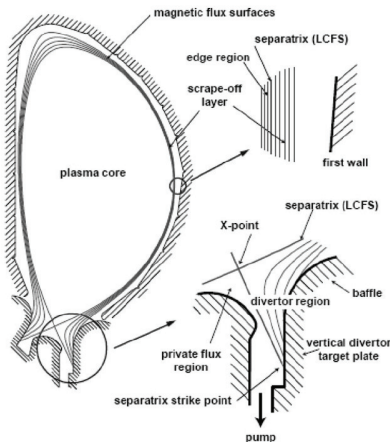


Figure: A poloidal cross-section of the magnetic configuration is shown on the left, whereas the plasma pressure from the core center to the edge is shown for the indicated radial arm



The edge defines a region of vastly different scales



core radius: $\sim 10^{-1} - 10^0$ m
 edge thickness: $\sim 10^{-3} - 10^{-2}$ m

Edge features

- last closed flux surface (LCFS): *separatrix*
- region outboard of LCFS: *scrape-off layer (SOL)*
- material boundaries (PFCs)
- *not* generally at LTE
- *not* guaranteed to be collisional (cf. next slide)

Image: Stangeby, P.C. *The Plasma Boundary of Magnetic Fusion Devices*. CRC Publishing, Bristol, England, United Kingdom, January 2000.



Edge region exhibits variability

	JET	C-mod
Parameters		
electron density n_e [m ⁻³]	10^{19}	$10^{20} - 10^{21}$
T_e [eV]	50	10
Connection length L [m]	40	8
$\nu_e^* = \nu_e / \nu_{e,bounce}$	25	1000
self-collisional mean free paths $\lambda_{ee}, \lambda_{ii}$ [m]	2.5	0.01
SOL dwell time $\tau_{SOL} = L/c_s$ [ms]	0.6	0.3

Table: Parameters in the scrape-off layer (SOL) for two tokamak devices.

Table: Stangeby, P.C. *The Plasma Boundary of Magnetic Fusion Devices*. CRC Publishing, Bristol, England, United Kingdom, January 2000.



Edge physics affects core confinement

- Edge conditions determine to a great extent the quality of confinement and dictate transport in the core.

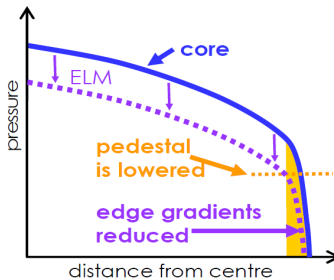
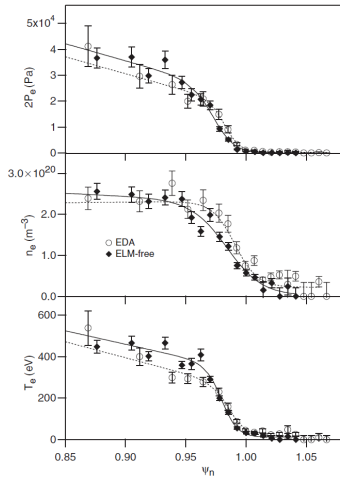
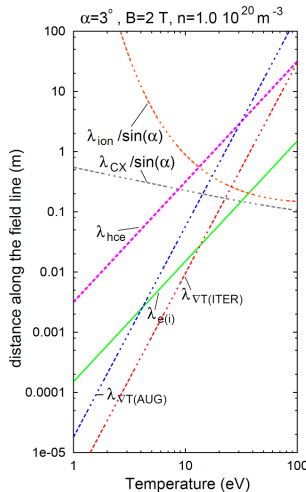


Figure: When any means (e.g. ELMs) causes removal of density from the edge region, the edge gradients decrease and so does the pedestal which directly reduces the confinement of the core.



The edge defines a region of vastly different scales



Left image: Stangeby, P.C. *The Plasma Boundary of Magnetic Fusion Devices*. CRC Publishing, Bristol, England, United Kingdom, January 2000., Right image: Mossessian, D. A. et al. *H-mode pedestal characteristics*



The utility of computer simulation



Computer simulations are indispensable in contributing to the understanding of magnetically confined plasmas

- Numerical simulations help guide experiments by
 - simulating and fine-tuning proposed experiments
 - producing results that have not yet been explored
 - post-processing can simulate diagnostic measurements
 - numerical solutions can aid design of devices (e.g. stellarators)
- Numerical simulations can access costly ventures (e.g. the *burning plasma* experiment)
- As more detailed and higher fidelity computational models are developed, the utility of computation increases and the feedback cycle becomes more efficient and useful.



Examples of contributions from computation

Computation contributes in manifold ways to theory/experiment:

- **Global stability and major disruption prevention:** By predicting the particular circumstances that cause them, e.g. Fredrickson, et al explained TFTR discharge collapse¹
 - Most energetically favorable configuration for that discharge caused relaxation to a long wavelength helical structure (nonlinear evolution to 3D equilibrium)
 - The resulting equilibrium aligns with the curvature of the device such that a pressure gradient is present in the bad curvature side
 - The local pressure bulge pushes outboard \Rightarrow stochasticization \Rightarrow thermal quench

¹E. Fredrickson, W. Park, et al, High-beta disruption in tokamaks



Examples of contributions from computation

Computation contributes in manifold ways to theory/experiment:

- **Design of three dimensional configurations:**

- Optimized 3D codes in N parameter space (e.g. 30~40 Fourier modes) can be used to explore magnetic topologies that meet desired transport, stability, and confinement requirements \Rightarrow **stellarators**²
- Examples: Quasi-poloidal compact stellarator (QPS) at ORNL, NCSX at PPPL³

²A. S. Ware et al., High-beta equilibria of drift-optimized compact stellarators, Phys.Rev. Lett. 89, 125503 (2002)

³Fusion simulation project (FSP): integrated simulation & optimization of fusion systems. December 1, 2002.



Examples of contributions from computation

Computation contributes in manifold ways to theory/experiment:

- **Computation has informed theory:**

- *Experiment:* H-mode is accompanied by abrupt increase in poloidal rotation in pedestal region.
- *Computation:* Turbulence can spontaneously generate large radial flows \Rightarrow transport barrier, agreement between gyrofluid and gyrokinetic codes!
- *Theory:* Experiment and numerical confirmations of Reynolds-stress-generated flows put on sound foundation through several analytical studies.

A. Hasegawa and M. Wakatani, Self-organization of electrostatic turbulence in a cylindrical plasma, Phys.Rev. Lett. 59, 1581 (1987).



Outline



Numerical challenges

① Multiple species: electrons, multiple ions, neutrals

② Time scales span $9 - 12$ orders of magnitude

- $\Omega_{ce}^{-1} \gtrsim 10^{-10}$ s : RF heating time scale
- $\tau \lesssim 10^2$ s : discharge time scale

③ Spatial scales span $4 - 6$ orders of magnitude

- $\lambda_{e,\nabla T} \gtrsim 10^{-5}$ m : ∇T length scale for electron conduction
- $L \lesssim 40$ m : connection length

④ Velocity scales span ~ 7 orders of magnitude

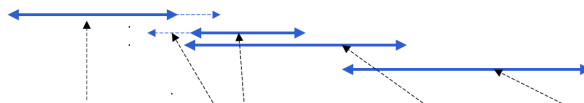
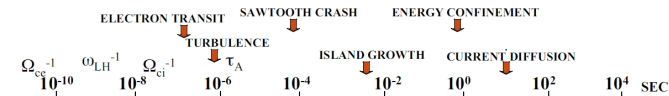
- $v_n \sim 0$ re-emitted neutrals adsorbed on wall
- $v_{Ti} \sim 36.12$ m/s for H^+ thermal ions $T_i = 0.025$ eV
- $v_{Te,SOL} \sim 10^6$ m/s for e^- in edge $T_e = 10 - 50$ eV
- $v_{Te} \sim 7.26 \times 10^7$ m/s for e^- at max $T_e \sim 30$ keV

Fully dimensional simulation requires 10^{11} phase space cells with 10^8 time steps over full discharge based on physical scales alone



The vastness in scales has motivated isolated codes

**Typical Time Scales in a next step experiment
with $B = 10$ T, $R = 2$ m, $n_e = 10^{14}$ cm $^{-3}$, $T = 10$ keV**



Single frequency and prescribed plasma background	Neglect displacement current, average over gyroangle, (some) with electrons	Neglect displacement current, integrate over velocity space, neglect electron inertia	Neglect displacement current, integrate over velocity space, average over surfaces, neglect ion & electron inertia
RF Codes wave-heating and current-drive	Gyrokinetics Codes turbulent transport	Extended MHD Codes device scale stability	Transport Codes discharge time-scale



Numerical challenges, cont'd

① Multiple collisional processes⁴:

- elastic: Coulomb (charged particles), Van der Waals (neutrals), charged particle - neutral momentum exchange
- inelastic: excitation, ionization, recombination, attachment, dissociation, etc.
- collision operator requires integral formulation in most cases

② Other challenges:

- long-range nature of EM forces \Rightarrow “grazing collisions”
- radiation transport \Rightarrow need opacity and emissivity feedback
- plasma-surface interaction
- if non-LTE, require atomic rate kinetics

⁴Güçlü, Y., et al. *Arbitrarily high-order semi-Lagrangian methods for the kinetic description of plasmas*, October 2, 2013



The need for deterministic semi-Lagrangian solutions

Deterministic solutions offer clear advantages:

- Statistical methods must simulate enough particles to resolve sparse regions \Rightarrow high computational cost
- Deterministic models can:
 - resolve high energy tail \Rightarrow accurate ionization rates
 - resolve electric fields in quasi-neutral regions; require no partitioning of scales

Alternative numerical solutions have disadvantages:

- **Eulerian** : strict time step requirement (CFL number), significant memory storage for a needed high resolution mesh
- **Lagrangian** : no CFL restriction, but require a Green's function to propagate solution.
- **Semi-Lagrangian** : no CFL restriction, trajectories pushed along known characteristic curves



Outline



Model equations

The plasma system is described by distribution functions for each particle species α :

$$f_\alpha = f_\alpha(t, \vec{x}, \vec{v}) : \mathbb{R}^+ \times \mathbb{R}^{d_x} \times \mathbb{R}^{d_v} \mapsto \mathbb{R}$$

the evolution of which is tied to the Boltzmann-Maxwell system:

$$\frac{\partial f_\alpha}{\partial t} + \vec{v} \cdot \frac{\partial f_\alpha}{\partial \vec{x}} + \frac{q_\alpha}{m_\alpha} (\vec{E} + \vec{v} \times \vec{B}) \cdot \frac{\partial f_\alpha}{\partial \vec{v}} = \left(\frac{\partial f_\alpha}{\partial t} \right)_{coll}$$

$$\epsilon_0 \vec{\nabla} \cdot \vec{E} = \sum_\alpha q_\alpha \int f_\alpha(t, \vec{x}, \vec{v}) d^3 \vec{v} \quad , \quad \vec{\nabla} \cdot \vec{B} = 0$$

$$\vec{\nabla} \times \vec{B} = \mu_0 \sum_\alpha q_\alpha \int \vec{v} f_\alpha(t, \vec{x}, \vec{v}) d^3 \vec{v} + \frac{1}{c^2} \frac{\partial \vec{E}}{\partial t} \quad , \quad \vec{\nabla} \times \vec{E} = - \frac{\partial \vec{B}}{\partial t}$$



Outline



Eulerian schemes

$$\frac{\partial f_\alpha}{\partial t} + \vec{v} \cdot \frac{\partial f_\alpha}{\partial \vec{x}} + \frac{q_\alpha}{m_\alpha} (\vec{E} + \vec{v} \times \vec{B}) \cdot \frac{\partial f_\alpha}{\partial \vec{v}} = \left(\frac{\partial f_\alpha}{\partial t} \right)_{coll}$$

- Distribution function $f_\alpha = f_\alpha(t, \vec{x}, \vec{v})$ lies on a fixed grid
- (t, \vec{x}, \vec{v}) are independent variables
- Derivatives are replaced with N th order finite differences
- Severe time step restriction (Courant-Friedrichs-Lowy, CFL) parameter to ensure stability

e.g. $|\mathcal{C}| := \left| \frac{v \Delta t}{\Delta x} \right| \leq \delta, \delta \in \mathbb{R}$

- usually requires the fine meshes with many phase space cells
 \Rightarrow large memory requirements and costly numerical solutions
- Examples: WENO, MUSCL



Lagrangian schemes

The distribution $f_\alpha = f_\alpha(t, \vec{x}(t), \vec{v}(t))$ is evolved in a moving frame:

$$\frac{df_\alpha}{dt} = \left(\frac{\partial f_\alpha}{\partial t} \right)_{coll}$$

defined by characteristics corresponding to particle trajectories:

$$\frac{d\vec{x}}{dt} = \vec{v}, \quad \text{and} \quad \frac{d\vec{v}}{dt} = \frac{q_\alpha}{m_\alpha} (\vec{E} + \vec{v} \times \vec{B})$$

Solution is obtained by computing

$$f_\alpha(t, \vec{x}, \vec{v}) = \int d\vec{x}' d\vec{v}' G(t, \vec{x}, \vec{v}; t', \vec{x}', \vec{v}') f_\alpha(t', \vec{x}', \vec{v}'), \quad t > t'$$

⇒ need Green's function for particular problem⁵

⁵Wichaidit, and Hitchon, W.N.G. *Propagator methods for plasma simulations: application ot breakdown*. J. Comput. Phys. 203 (2005) p.650–667



Outline



Semi-Lagrangian methods

The distribution $f_\alpha = f_\alpha(t, \vec{x}, \vec{v})$ lies on a fixed grid. Two steps:

- ① Eulerian step: Update velocities according to collisions on fixed grid:

$$\frac{\partial f_\alpha}{\partial t} = \left(\frac{\partial f_\alpha}{\partial t} \right)_{coll}$$

- ② Lagrangian step: Solve collisionless equation on Lagrangian mesh:

$$\frac{df_\alpha}{dt} = 0$$

by convecting $f_\alpha(t, \vec{x}, \vec{v})$ along characteristics over a step Δt

$$\frac{d\vec{x}}{dt} = \vec{v}, \quad \text{and} \quad \frac{d\vec{v}}{dt} = \frac{q_\alpha}{m_\alpha} (\vec{E} + \vec{v} \times \vec{B})$$

Remap $f_\alpha(t + \Delta t, \vec{x}, \vec{v})$ to Eulerian mesh

Examples: Cheng and Knorr, CS, discontinuous Galerkin



Outline



Classic convected scheme

- ② Lagrangian step: convect $f_\alpha(t_0, \vec{x}_0, \vec{v}_0) \rightarrow f_\alpha(t, \vec{x}, \vec{v})$ along characteristics:

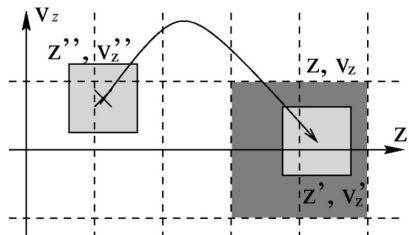
$$\frac{d\vec{x}}{dt} = \vec{v}, \quad \text{and} \quad \frac{d\vec{v}}{dt} = \frac{q_\alpha}{m_\alpha} (\vec{E} + \vec{v} \times \vec{B})$$

Remap $f_\alpha(t, \vec{x}, \vec{v})$ to Eulerian mesh

Moving cell (MC) is a control volume:

$$\int_{MC(t)} f(t, \vec{x}, \vec{v}) d^3\vec{x} d^3\vec{v}$$

$$= \int_{MC(t_0)} f(t_0, \vec{x}_0, \vec{v}_0) d^3\vec{x}_0 d^3\vec{v}_0$$



If f_{MC} is constant \Rightarrow Remap to each cells at (\vec{x}, \vec{v}) according to cell volume overlap

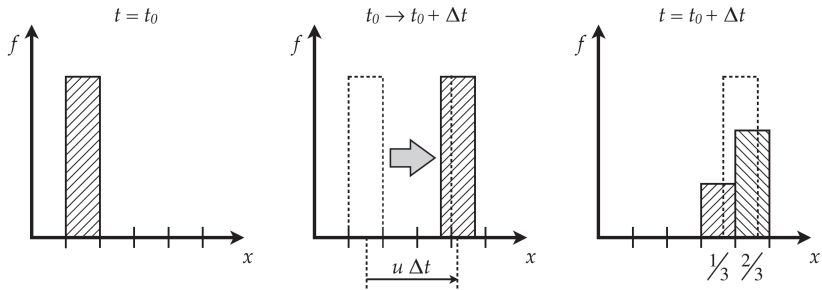


Outline



High order convected scheme: motivation

Problem: remapping assignment has $\mathcal{O}(\Delta x^2)$ error



Through modified equation analysis⁶ this error is identified as numerical diffusion

⁶Image: Güçlü, Y. et al. A high order cell-centered semi-Lagrangian scheme for multidimensional kinetic simulations of neutral gas flows. J. Comput. Phys. 231 (2012)



Higher order convected scheme

The 1D constant advection equation ($v \geq 0$) is given by

$$\frac{\partial f}{\partial t} + v \frac{\partial f}{\partial x} = 0$$

The CS update from time $t^n = n\Delta t \rightarrow t^{n+1}$ is found to be

$$(f_{i+S}^{n+1})_{\text{CS}} = \alpha_{i-1}^n f_{i-1}^n + (1 - \alpha_i^n) f_i^n$$

Where the number of cells (width Δx) travelled is

$$C := \frac{v\Delta t}{\Delta x} = S + \alpha, \quad S \in \mathbb{N}, \alpha \in [0, 1)$$



Higher order convected scheme

High order CS seeks a correction $\alpha \rightarrow U^7$:

$$U(t, x) = [v + \tilde{v}] \frac{\Delta t}{\Delta x} = \alpha + \tilde{\alpha}(t, x)$$

$\tilde{\alpha}$ is an *anti-diffusive* correction. The corrected CS update reads:

$$(f_{i+S}^{n+1})_{\text{CS}} = U_{i-1}^n f_{i-1}^n + (1 - U_i^n) f_i^n$$

We find order conditions by matching expansions about (x_i, t^n) of the exact solution with the CS solution

⁷This stepthrough was developed by Güçlü, Y., et al. *Arbitrarily high order convected scheme solution of the Vlasov-Poisson system*. J. Comput. Phys. **270**, 0 (2014), p.711-752.



Higher order convected scheme

Find order conditions:

- Expand the exact solution $f(t + \Delta t, x) = f(t, x - v\Delta t)$ noting $v\Delta t = \alpha\Delta x$:

$$(f_{i+S}^{n+1})_{\text{exact}} = f(t, x) + \sum_{p=1}^N \alpha^p \frac{(-\Delta x)^p}{p!} \frac{\partial^p f}{\partial x^p} \Big|_{(t,x)} + \mathcal{O}(\Delta x^{N+1})$$

- Expanding $U_{i-1}^n f_{i-1}^n = U(t, x - \Delta x) f(t, x - \Delta x)$ in the CS update, we find

$$(f_{i+S}^{n+1})_{\text{CS}} = f(t, x) + \sum_{p=1}^N \frac{(-\Delta x)^p}{p!} \frac{\partial^p (Uf)}{\partial x^p} \Big|_{(t,x)} + \mathcal{O}(\Delta x^{N+1})$$



Higher order convected scheme

Correct so that the local truncation error (LTE) is correct up to order N :

$$\text{LTE}(t, x, \Delta x) := f_{\text{exact}}(t + \Delta t, x + S\Delta x) - f_{\text{CS}}(t + \Delta t, x + S\Delta x) = \mathcal{O}(\Delta x^{N+1})$$

This requires

$$\sum_{p=1}^N \frac{(-\Delta x)^p}{p!} \alpha^p \frac{\partial^p f}{\partial x^p} \Big|_{(t,x)} - \sum_{p=1}^N \frac{(-\Delta x)^p}{p!} \frac{\partial^p (Uf)}{\partial x^p} \Big|_{(t,x)} = 0$$



Higher order convected scheme

To proceed further, assert a form for Uf :

$$U(t, x)f(t, x) := \sum_{q=0}^{N-1} \beta_q(\alpha)(-\Delta x)^q \frac{\partial^q f}{\partial x^q} \Big|_{(t,x)} + \mathcal{O}(\Delta x^{N+1})$$

Inserting these into the above order conditions, closed form solutions for each coefficient function β are found:

$$\beta_p(\alpha) = \frac{\alpha^{p+1}}{(p+1)!} - \sum_{q=0}^{p-1} \frac{\beta_q(\alpha)}{(p+1-q)!}, \quad p = 1, 2, \dots$$

and $\beta_0 = \alpha$.



Higher order convected scheme

Thus, the following permit calculation of the correction flux Uf to order N :

$$U(t, x)f(t, x) := \sum_{q=0}^{N-1} \beta_q(\alpha)(-\Delta x)^q \frac{\partial^q f}{\partial x^q} \Big|_{(t,x)}$$

$$\beta_p(\alpha) = \frac{\alpha^{p+1}}{(p+1)!} - \sum_{q=0}^{p-1} \frac{\beta_q(\alpha)}{(p+1-q)!}, \quad p = 1, 2, \dots$$

with $\beta_0 = \alpha = C - S$.

The method of how the $N - 2$ derivatives are computed delineates two methods of high order CS:

- **FDN** : derivatives are calculated by finite differences
- **FN** : derivatives are calculated in Fourier space

Here, the the marker N denotes the order of accuracy (e.g. FD5 is a 5th order CS method corrected by finite difference calculations).





Outline



Split operator methods

Higher dimensional PDE model case: the **Vlasov equation**

$$\frac{\partial f_\alpha}{\partial t} + v \frac{\partial f_\alpha}{\partial x} + \frac{q_\alpha E}{m_\alpha} \frac{\partial f}{\partial v} = 0$$

Define the Hamiltonian $H = \frac{m_\alpha v^2}{2} + q_\alpha \phi(x)$, then the Vlasov equation is equivalently

$$\frac{\partial f_\alpha}{\partial t} = \frac{1}{m_\alpha} \{H, f_\alpha\} \equiv \Lambda f_\alpha$$

Λ is the *Liouvillian operator*. Since the PDE does not explicitly depend on time, The exact solution after $t \in [0, \tau]$ is given by:

$$f_\alpha(\tau, x, v) = e^{\tau \Lambda} f_\alpha(0, x_0, v_0) = T^\tau f_\alpha(0, x_0, v_0)$$

T^τ is a time evolution operator:

$$T^\tau = e^{\tau \Lambda} = e^{\tau \Lambda_x + \tau \Lambda_v}$$



Split operator methods

The form of the total time evolution operator is not known; however, we will see it can be decomposed into sub-operators we **do** know

Operator splitting: to partition an operator into several parts whose compositional action approximates the original operator

Here, we consider how to parse the time evolution operator

$T^\tau = e^{\tau\Lambda}$, where

$$\Lambda = m_\alpha^{-1}\{H, \cdot\} = m_\alpha^{-1}\{H_T + H_V, \cdot\} = m_\alpha^{-1}\{H_T, \cdot\} + m_\alpha^{-1}\{H_V, \cdot\} = \Lambda_x + \Lambda_v$$

is an exact partition; however, the exponential splitting incurs some error:

$$T^\tau = e^{\tau\Lambda} = e^{\tau\Lambda_x + \tau\Lambda_v} = e^{\tau\Lambda_x} e^{\tau\Lambda_v} + \mathcal{O}(\tau^2)$$

Problem: need to know the form or action of these sub-operators $(e^{\tau\Lambda_x}, e^{\tau\Lambda_v})$ to use them



Split operator methods

Solution: the action of these operators = convection along characteristics!

$$\begin{aligned}\frac{\partial f_\alpha}{\partial t} + v \frac{\partial f_\alpha}{\partial x} + \frac{q_\alpha E}{m_\alpha} \frac{\partial f}{\partial v} &= 0 \\ \frac{\partial f_\alpha}{\partial t} - \underbrace{\frac{1}{m_\alpha} \{H_T(v), f_\alpha\}}_{=\Lambda_x f_\alpha} - \underbrace{\frac{1}{m_\alpha} \{H_V(x), f_\alpha\}}_{=\Lambda_v f_\alpha} &= 0\end{aligned}$$

The Vlasov equation is equivalent to

$$\frac{\partial f_\alpha}{\partial t} - \Lambda_x f_\alpha - \Lambda_v f_\alpha = 0$$

And, these operators are used to solve the split problems

$$\frac{\partial f_\alpha}{\partial t} - v \frac{\partial f_\alpha}{\partial x} = 0 \quad \Rightarrow f_\alpha(\tau, x, v) = e^{\tau \Lambda_x} f_\alpha(0, x, v) = f_\alpha(0, x - v\tau, v)$$

$$\frac{\partial f_\alpha}{\partial t} - \frac{q_\alpha E}{m_\alpha} \frac{\partial f}{\partial v} = 0 \quad \Rightarrow f_\alpha(\tau, x, v) = e^{\tau \Lambda_v} f_\alpha(0, x, v) = f_\alpha(0, x, v - \frac{q_\alpha E}{m_\alpha} \tau)$$



Split operator methods

Thus, multidimensional equations

$$\frac{\partial f_\alpha}{\partial t} + v \frac{\partial f_\alpha}{\partial x} + \frac{q_\alpha E}{m_\alpha} \frac{\partial f}{\partial v} = 0$$

can be split into simple 1D advection equations in phase space:

$$\frac{\partial f_\alpha}{\partial t} - v \frac{\partial f_\alpha}{\partial x} = 0 \Rightarrow f_\alpha(\tau, x, v) = e^{\tau \Lambda_x} f_\alpha(0, x, v) \equiv \mathcal{X}^\tau f_\alpha(0, x, v)$$

$$\frac{\partial f_\alpha}{\partial t} - \frac{q_\alpha E}{m_\alpha} \frac{\partial f}{\partial v} = 0 \Rightarrow f_\alpha(\tau, x, v) = e^{\tau \Lambda_v} f_\alpha(0, x, v) \equiv \mathcal{V}^\tau f_\alpha(0, x, v)$$

whose solutions are computed through high order CS, though at the cost of a time error $\mathcal{O}(\tau^N)$



Split operator methods

Notation summary:

$$\underline{\text{Exact operator in } (x, v) : \quad T^\tau = e^{\tau(\Lambda_x + \Lambda_v)}}$$

$$\underline{\text{Split operator in } x : \quad X^\tau = e^{\tau \Lambda_x}}$$

$$\underline{\text{Split operator in } v : \quad V^\tau = e^{\tau \Lambda_v}}$$

A first order splitting:

$$T^\tau f_\alpha(\tau, x, v) = X^\tau \circ V^\tau f_\alpha(0, x, v) + \mathcal{O}(\tau^2)$$

In general, we can seek coefficients that describe fractional time steps c_i, d_i so that the above equation is order N accurate:

$$T^\tau = \prod_{i=1}^s X^{c_i \tau} V^{d_i \tau} + \mathcal{O}(\tau^{N+1}), \quad \sum_i c_i = \sum_i d_i = 1$$

Preliminary work



Verifying numerical order of accuracy

- For an N th order method, the *local truncation error* (LTE) for a mesh with spacing Δx is:

$$\text{LTE}_{\Delta x} = \mathcal{O}(\Delta x^{N+1})$$

- The global error (GE) accumulated over the simulation time $0 \leq t \leq T$ with $N_t = T/\Delta t$ time steps is then:

$$N_t \cdot \text{LTE}_{\Delta x} = N_t \cdot \mathcal{O}(\Delta x^{N+1}) = \frac{T}{\Delta t} \cdot \mathcal{O}(\Delta x^{N+1}) \sim \mathcal{O}(\Delta x^{N+1}/\Delta t)$$

- We fix the CFL number so that the errors are simply related:

$$\mathcal{C} = v\Delta t/\Delta x \Rightarrow \mathcal{O}(\Delta t) = \mathcal{O}(\Delta x)$$

- Thus, the global error calculated is expected to be

$$\text{GE}_{\Delta x} = \mathcal{O}(\Delta x^N)$$

for an N th order method



Verifying numerical order of convergence, cont'd

- We consider the normalized root-mean-square (NRMS) of the L^2 error norm averaged over the domain length $|\mathcal{D}| = L$. The global error (GE) at end of simulation $t = T$ is given by:

$$\text{NRMS}(\text{GE}_{\Delta x}) = \frac{1}{\sqrt{L}} \left[\sum_{i=0}^{N_x-1} [f_{\text{CS}}(T, x_i) - f_{\text{exact}}(T, x_i)]^2 \Delta x \right]^{1/2}$$

- It can be shown that the order N is calculated according to:

$$N := \log_2 \left(\frac{\overline{\text{GE}}_{\Delta x}}{\overline{\text{GE}}_{\Delta x/2}} \right), \quad \Delta x \rightarrow 0$$

Thus, refining the mesh $\Delta x \rightarrow \Delta x/2 \rightarrow \Delta x/4 \rightarrow \dots$ converges on the order N



Verifying numerical order of accuracy, cont'd

Model problem: 1D uniform speed advection solutions

- We solve the 1D unit velocity ($v = 1$) advection equation subject to a periodic boundary condition:

$$\frac{\partial f}{\partial t} + \frac{\partial f}{\partial x} = 0, \quad x \in \mathcal{D}, t \in [0, T]$$

$$f(0, x) = f_0(x)$$

$$f(t, x + L) = f(t, x)$$

- For a grid described by:

$$N_x = \frac{|\mathcal{D}|}{\Delta x} \quad \text{spatial cells}$$

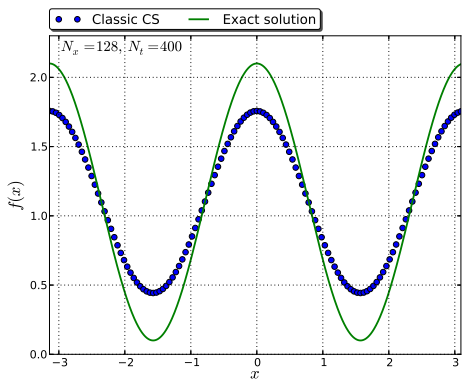
$$N_t = \frac{T}{\Delta t} \quad \text{time steps}$$



Classic CS: convergence analysis

A classic CS method has been implemented for

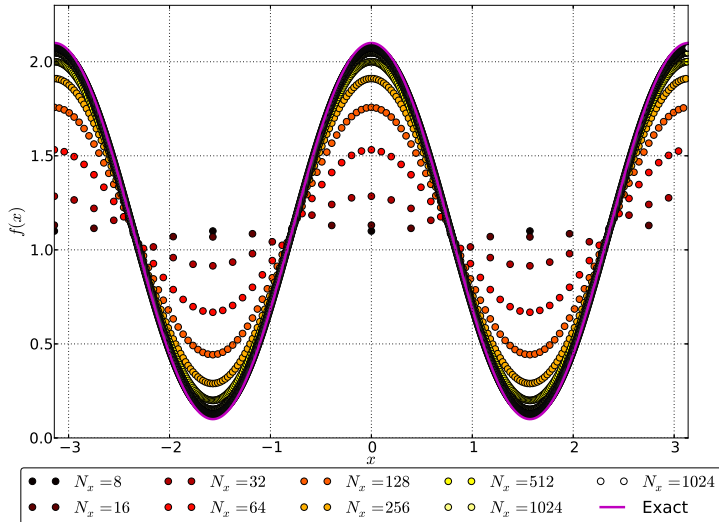
$$f_0(x) = 1.1 + \cos(2x), \quad x \in \mathcal{D} = [-\pi, \pi], \quad t \in [0, 2\pi]$$



Classic CS		
	NRMS(GE $_{\Delta x}$)	Order
N_x		
32	1.4448	—
64	1.0073	0.5204
128	6.0739×10^{-1}	0.7298
256	3.3537×10^{-1}	0.8569
512	1.7646×10^{-1}	0.9264
1024	9.0539×10^{-2}	0.9626
2048	4.5863×10^{-2}	0.9812



Classic CS: mesh refinement results ($CFL = 0.32$)





Classic CS: demonstration

[show movie: plot_--cos2x_ClassicCS_Nx64Nt200.mpeg and
plot_--cos2x_ClassicCS_Nx1024Nt3200.mpeg]

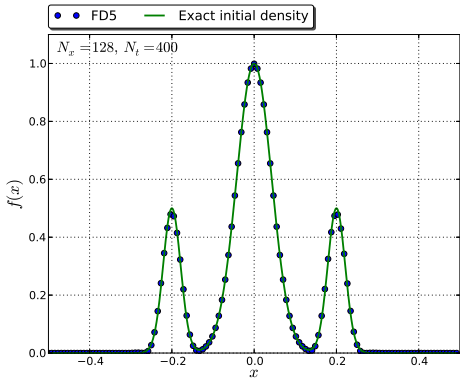


Higher order CS (*FD5*): convergence analysis

A 5th order CS method with finite differences (*FD5*) has been implemented:

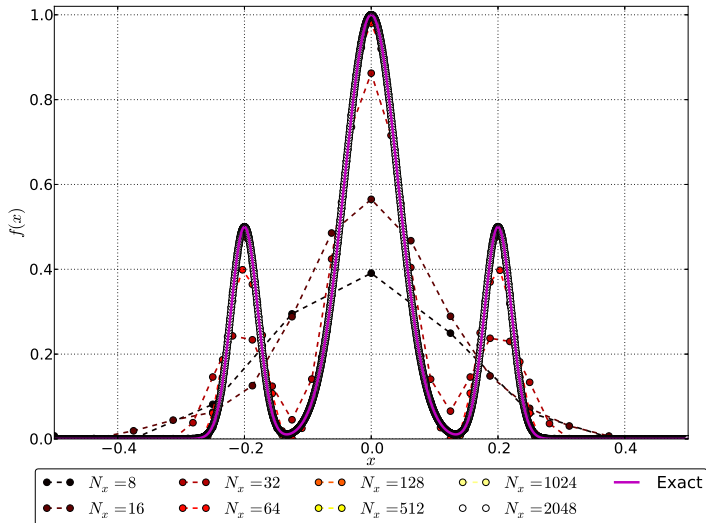
$$f_0(x) = \frac{1}{2}e^{-\left(\frac{x+0.2}{0.03}\right)^2} + e^{-\left(\frac{x}{0.06}\right)^2} + \frac{1}{2}e^{-\left(\frac{x-0.02}{0.03}\right)^2}$$

FD5		
	NRMS(GE $_{\Delta x}$)	Order
N_x		
32	7.2912×10^{-2}	—
64	2.5443×10^{-2}	1.5189
128	4.4472×10^{-3}	2.5163
256	2.1447×10^{-4}	4.3741
512	7.0343×10^{-6}	4.9302
1024	2.2142×10^{-7}	4.9895
2048	6.9307×10^{-9}	4.9976





Higher order CS (FD5): mesh refinement ($\mathcal{C} = 0.32$)



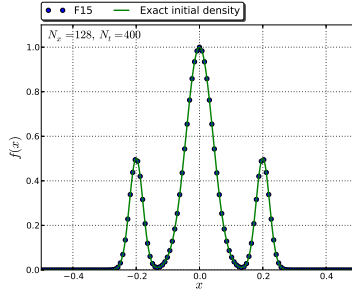
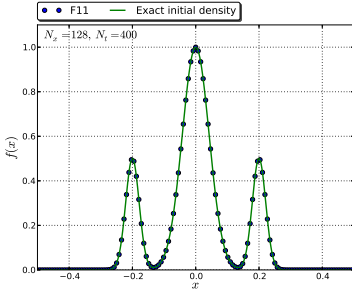
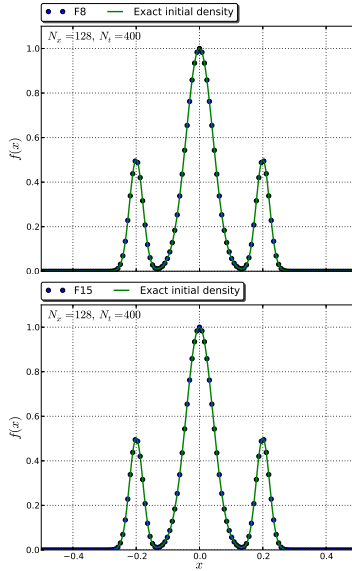
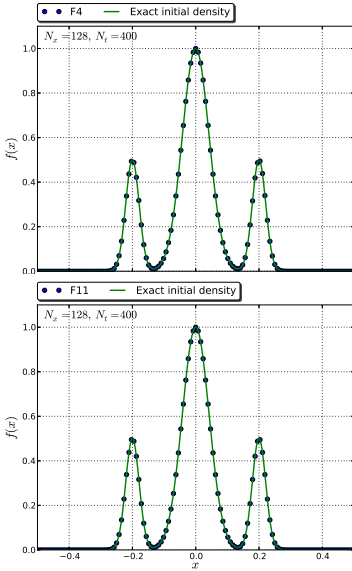


Higher order CS (*FD5*): demonstration

[show movie: plot_--GB3_FD5_Nx128Nt400.mpeg]



Higher order CS (*FN* methods): various orders N



<i>F2</i>		<i>F3</i>		<i>F4</i>	
NRMS(GE _{Δx})	Order	NRMS(GE _{Δx})	Order	NRMS(GE _{Δx})	Order
<i>N_x</i>					
32	9.3763×10^{-2}	–	5.3484×10^{-2}	–	2.1076×10^{-2}
64	4.7483×10^{-2}	0.9816	1.9892×10^{-2}	1.4269	4.9206×10^{-3}
128	2.06645×10^{-2}	1.2003	4.4207×10^{-2}	2.1698	3.6497×10^{-4}
256	6.170×10^{-3}	1.7436	6.2759×10^{-4}	2.8163	2.2817×10^{-5}
512	1.5708×10^{-3}	1.9739	8.0046×10^{-5}	2.9709	1.4228×10^{-6}
<i>F5</i>		<i>F6</i>		<i>F7</i>	
NRMS(GE _{Δx})	Order	NRMS(GE _{Δx})	Order	NRMS(GE _{Δx})	Order
<i>N_x</i>					
32	1.8251×10^{-2}	–	1.4003×10^{-2}	–	1.3743×10^{-2}
64	2.0776×10^{-3}	3.1350	4.7357×10^{-4}	4.8860	2.2053×10^{-4}
128	8.0741×10^{-5}	4.6855	7.7235×10^{-6}	5.9381	1.9207×10^{-6}
256	2.5658×10^{-6}	4.9757	1.1945×10^{-7}	6.0147	1.5166×10^{-8}
512	8.0364×10^{-8}	4.9967	1.8608×10^{-9}	6.0042	–
<i>F8</i>		<i>F9</i>		<i>F10</i>	
NRMS(GE _{Δx})	Order	NRMS(GE _{Δx})	Order	NRMS(GE _{Δx})	Order
<i>N_x</i>					
32	1.3757×10^{-2}	–	1.3711×10^{-2}	–	1.3742×10^{-2}
64	5.6229×10^{-5}	7.934635	3.0591×10^{-5}	8.808078	1.4822×10^{-5}
128	2.1371×10^{-7}	8.039495	5.8963×10^{-8}	9.019098	7.3664×10^{-9}
256	8.2396×10^{-10}	8.039495	1.1657×10^{-10}	8.982388	7.0799×10^{-12}
512	–	–	–	–	1.0180×10^{-13} (<i>m.p.</i>)

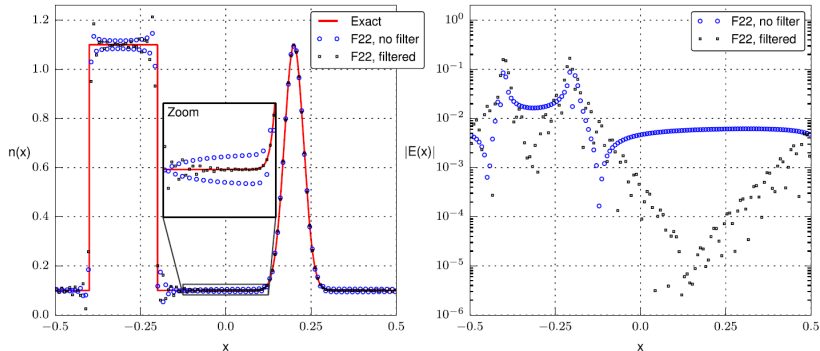
<i>F</i> 11			<i>F</i> 12			<i>F</i> 13		
	NRMS(GE _{Δx})	Order		NRMS(GE _{Δx})	Order		NRMS(GE _{Δx})	Order
<i>N_x</i>								
32	1.3733×10^{-2}	–		1.3736×10^{-2}	–		1.3734×10^{-2}	–
64	1.3397×10^{-5}	10.0014		1.2761×10^{-5}	10.0721		1.2718×10^{-5}	10.0766
128	2.2175×10^{-9}	12.5607		3.0450×10^{-10}	15.3548		9.8644×10^{-11}	16.9763
256	1.1011×10^{-12}	10.9758		9.7125×10^{-14}	(<i>m.p.</i>)		6.7652×10^{-14}	(<i>m.p.</i>)
512	1.0180×10^{-13}	(<i>m.p.</i>)		1.0187×10^{-13}	(<i>m.p.</i>)		1.0182×10^{-13}	(<i>m.p.</i>)

Accuracy achieves machine precision (*m.p.*) too soon for higher orders to be confirmed



Challenge case: juxtaposition of all schemes

Sharp boundaries present challenges to adequately resolve⁸



A windowed Fourier transform (WFT) can be applied to localize the jump errors (cf. preliminary document)

⁸Güçlü, Y., et al. *Arbitrarily high order convected scheme solution of the Vlasov-Poisson system*. J. Comput. Phys. **270**, 0 (2014), p.711-752.



1D variable velocity advection solutions

We now permit the velocity to vary as a function of position

$$\frac{\partial f}{\partial t} + v(x) \frac{\partial f}{\partial x} = 0, \quad x \in \mathcal{D}, t \in [0, T]$$

$$f(0, x) = f_0(x)$$

$$f(t, x + L) = f(t, x)$$

And analyze the initial Gaussian distribution:

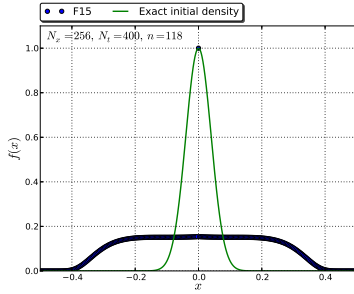
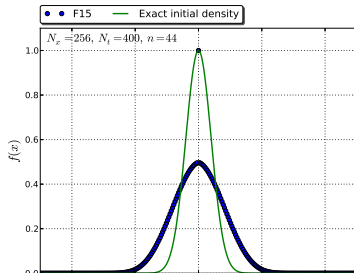
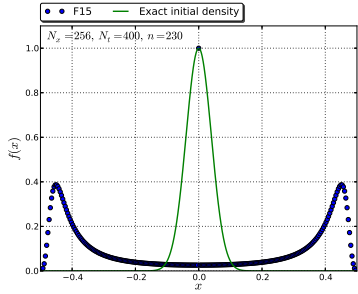
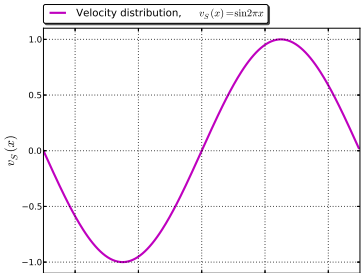
$$f_0(x) = e^{-x^2/(2(0.04)^2)}, \quad x \in [-0.5, 0.5]$$

With prescribed velocity field:

$$v_S(x) = \sin 2\pi x$$



Variable velocity: snapshots





Variable velocity: demonstration

[show movie: N_v_S_F8_Nx256Nt400.mpeg]



Operator splitting methods

Four split methods were implemented:

- **LF2** – 2nd order, 1 stage (*Leapfrog or Strang scheme*)
- **Y4** – 4th order, 3 stages (*Yoshida scheme*)
- **O6-4** – 6th order, optimized, 6 stages (*optimized*)
- **O11-6** – 6th order, optimized, 11 stages (*optimized*)

Yoshida, H. *Construction of higher order integrators*. Physics letters **150**, 5,6,7 (1990)

Blanes, S. et al. *Practical symplectic partitioned Runge-Kutta and Runge-Kutta-Nyström methods*. J. Comput. and App. Mathe. **143**, 313–330



2D rotating advection equation

We analyze a 2D rotating advection problem:

$$\frac{\partial f}{\partial t} + 2\pi y \frac{\partial f}{\partial x} - 2\pi x \frac{\partial f}{\partial y} = 0$$

$$(x, y) \in [-1, 1] \times [-1, 1], \quad t \in [0, 1]$$

$$f(t, x + L, y) = f(t, x, y), \quad f(t, x, y + L) = f(t, x, y)$$

i.e. the velocities are spatially dependent:

$$v_x(x, y) = 2\pi y, \quad v_y(x, y) = -2\pi x$$

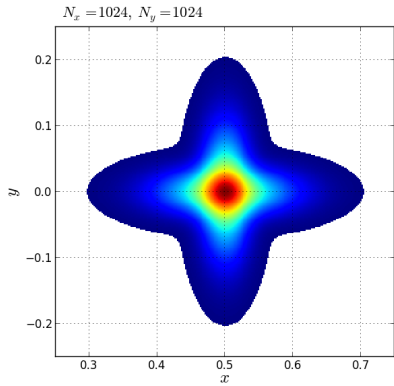
which describes rotation about $(x_0, y_0) = (0, 0)$ with constant angular velocity $\omega = 2\pi$ and period 1.



2D rotating advection: initial distribution

The initial distribution we consider is:

$$f_0(x, y) = 0.5B(r_1(x, y)) + 0.5B(r_2(x, y))$$



$$B(r, a) = \begin{cases} \cos^2\left(\frac{\pi r}{2a}\right) & \text{for } r \leq a \\ 0 & \text{else} \end{cases}$$

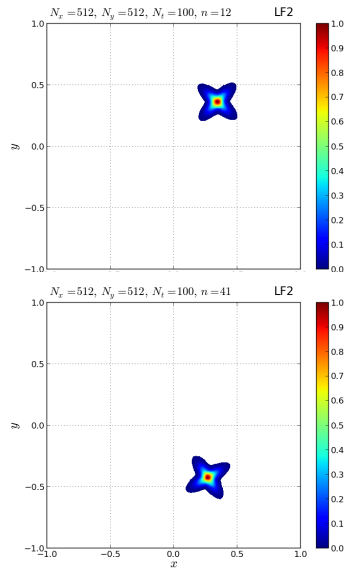
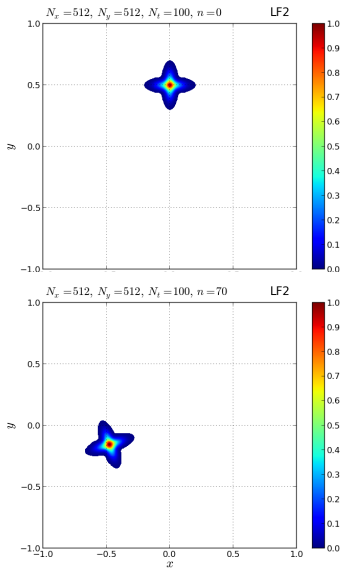
$$r_1(x, y) = \sqrt{(x - x_c)^2 + 8(y - y_c)^2}$$

$$r_2(x, y) = \sqrt{8(x - x_c)^2 + (y - y_c)^2}$$

$$2a = 1, \quad (x_c, y_c) = (0, 0.5)$$



2D rotating advection: snapshots





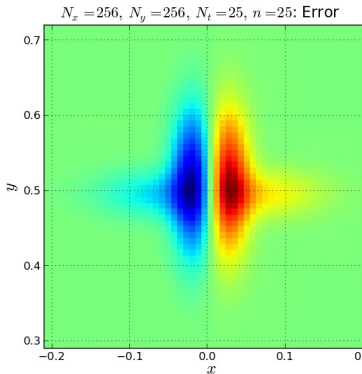
2D rotating advection: errors in different split schemes

[show movie: plot_-_flower_F12_LF2_Nx512Nt100.mpeg]



2D rotating advection: errors in different split schemes

The NRMS(GE $_{\Delta x, \Delta y}$) in 2D is the Frobenius norm $\|\cdot\|_F$ normalized by the area $|\mathcal{D}_x||\mathcal{D}_y|$. CS solver was the *F12* scheme.



NRMS(GE $_{\Delta x, \Delta y}$)

Scheme	
<i>LF2</i>	4.5338×10^{-3}
<i>Y4</i>	1.4368×10^{-3}
<i>O6-4</i>	2.1483×10^{-5}
<i>O11-6</i>	3.9634×10^{-7}



1D-1V Vlasov equation: prescribed \vec{E} -field

Setup:

- Trapped electrons ($q = -e$) are simulated in a prescribed electric (\vec{E}) field as governed by the Vlasov equation.
- normalize according to
 - $t \rightarrow t/\tau$, where $\tau^{-1} = \omega_{pe}/2\pi$
 - $x \rightarrow x/\lambda_D$
 - $v \rightarrow v/v_{Te} = v/(\lambda_D \omega_{pe})$
 - $E \rightarrow E/\bar{E}$, where $\bar{E} = \frac{1}{2}m_e v_{Te}^2/q \cdot \omega_{pe}$
 - $f \rightarrow f/\bar{f}$, where $\bar{f} = \langle f \rangle_v / v_{Te}^3$
- Recall $E = -\partial_x \phi$

Then the Vlasov equation takes the form:

$$\frac{\partial f}{\partial t} + v \frac{\partial f}{\partial x} + \frac{\partial \phi}{\partial x} \frac{\partial f}{\partial v} = 0$$

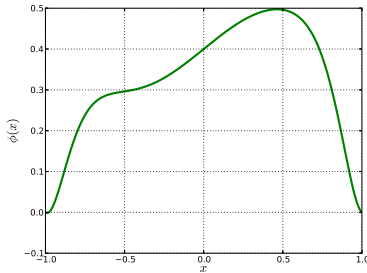
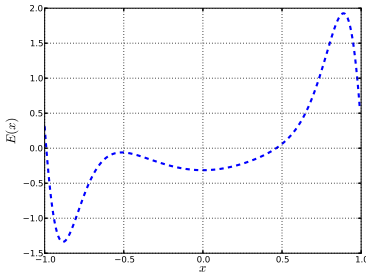


1D-1V Vlasov equation: prescribed \vec{E} -field

$$\frac{\partial f}{\partial t} + v \frac{\partial f}{\partial x} + \frac{\partial \phi}{\partial x} \frac{\partial f}{\partial v} = 0$$

Trapped electrons are simulated with the *F12* CS by considering the potential:

$$\phi(x) = 0.2 + 0.2 \cos(\pi x^4) + 0.1 \sin(\pi x)$$



over a simulation time $0 \leq t \leq 6.4$

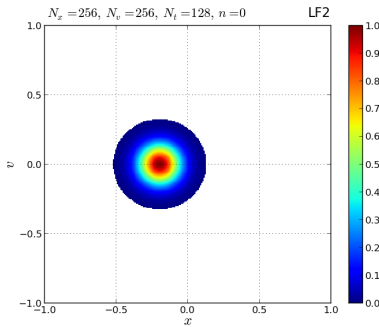


1D-1V Vlasov equation: prescribed \vec{E} -field

Initial distribution

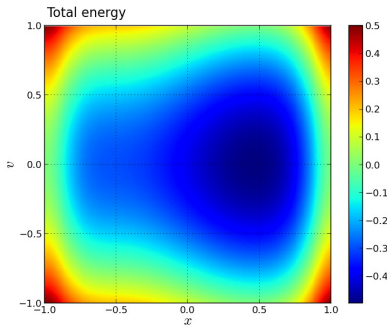
$$B(r, a) = \begin{cases} \cos^{22} \left(\frac{\pi r}{2a} \right) & \text{for } r \leq a \\ 0 & \text{else} \end{cases}$$

$$r = \sqrt{(x - x_c)^2 + (v - v_c)^2}$$



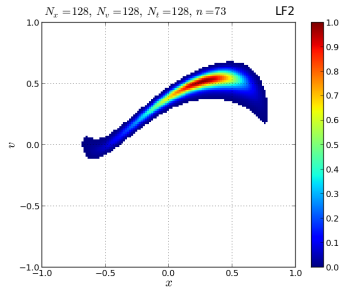
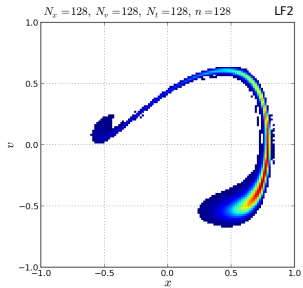
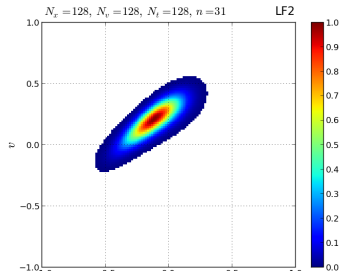
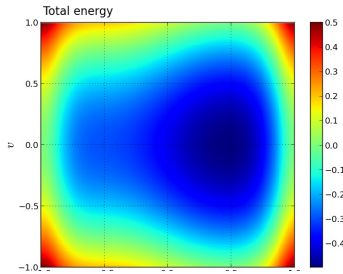
The Hamiltonian is constant:

$$H = \frac{1}{2}v_0^2 - \phi(x_0) = \frac{1}{2}v(t)^2 - \phi(x(t))$$





1D-1V Vlasov equation: prescribed \vec{E} -field, snapshots





1D-1V Vlasov equation: prescribed \vec{E} -field: demonstration

[show movie: plot_--1DVP_F12_Nx256Nv256Nt256.mpeg]

Proposed work



1D-1V Vlasov-Poisson system

- We aim to extend the code to calculate electric field self-consistently

$$\partial_t f + v \partial_x f = 0, \quad \epsilon_0 \partial_x^2 \phi = -q \int dv f(t, x, v)$$

- Will benchmark with bump-on-tail instability and Landau damping test cases as obtained by:
 - Discontinuous Galerkin:** Rossmanith, J. A. and Seal, D.C. *A positivity-preserving high-order semi-Lagrangian discontinuous Galerkin scheme for the Vlasov-Poisson equations.* J. Comput. Phys. **230**, 16 (2011), p.6203–6232
 - Finite difference:** T. Zhou, Y. Guo., et al. *Numerical study on Landau damping.* Phys. D Nonlinear Phenom. **157** (2001) p.322-333.
 - Convected scheme:** Güçlü, Y., et al. *Arbitrarily high order convected scheme solution of the Vlasov-Poisson system.* J. Comput. Phys. **270**, 0 (2014), p.711-752.



Boundaries

Boundary region (\sim mm thick) modeling challenges:

- sharp gradients in parameters (n, T, ϕ)
- vast scales and sparsity in phase space
- discontinuity at wall

We plan to seek high order solutions as a two-step procedure:

- ① local mesh refinement near wall (*multiple scales of resolution*)
⇒ will require extending high order CS to nonuniform meshes
- ② Employ an artificial compression method (ACM, or *Harten*) filter to sharpen the above solution to simulate the cutoff⁹

⁹Harten, A. *The artificial compression method for computation of shocks and contact discontinuities: III. Self-adjusting hybrid schemes* Mathematics of Computation **32**, 142 (1978), p.363–389



Collisions

The chosen collision operator $\left(\frac{\partial f_\alpha}{\partial t}\right)_{coll} \equiv C_{\alpha\beta}(f_\alpha, f_\beta)$ presents variable complexity

- *Bhatnagar-Gross-Krook (BGK) operator:*

$$C_{\alpha\alpha}^{BGK}(f_\alpha) = \nu^{\alpha/\alpha}(v_\alpha)(f_\alpha - f_\alpha^{Maxwellian})$$

Many realistic scenarios require integral representations:

- Lorentz collision operator ($m_\beta \gg m_\alpha$)
- Fokker-Planck collisions ($\Delta\theta \ll 1$)
- Boltzmann collision integral
- Landau collision operator $C_{\alpha\beta}^L$

$$C_{\alpha\beta}^L = \frac{\partial}{\partial \vec{v}_\alpha} \cdot \int_{\mathbb{R}^N} d\vec{v}_\beta a(\vec{v}_\alpha - \vec{v}_\beta) [f_\beta \frac{\partial f_\alpha}{\partial \vec{v}_\alpha} - f_\alpha \frac{\partial f_\beta}{\partial \vec{v}_\beta}]$$

- need a high order and efficient means of calculating based on high order solutions from coarser meshes \Rightarrow **integral deferred correction (IDC)** by correction loops.



Collisions, cont'd

Integral deferred correction (IDC)¹⁰ methods will be investigated as a predictor-corrector strategy to include high order accurate solutions with collisions

Each time step is partitioned into m substeps:

$$[t^n, t^{n+1}] \Rightarrow t^n = t^{n,0} < \dots < t^{n,m-1} = t^{n+1}$$

and loop through the following procedure for $k = 0, 1, \dots, m - 1$ for the provisional solution $f(t^{n,k})$ ¹¹:

- ① Estimate the error according to IDC
- ② Evolve the error equation for $\delta^k \mapsto \delta^{k+1}$
- ③ Correct the solution $f(t^{n,k+1}) = f(t^{n,k}) + \delta^{k+1}$

¹⁰Christlieb, A., et al. *Integral deferred correction methods constructed with high-order Runge-Kutta integrators*. Mathematics of Computation (March 2009).

¹¹arXiv:1310.6015v2



Collisions, cont'd

We will apprehend collisions through the following models

- BGK operator ($\alpha, \beta = e, i, n$): $C_{\alpha\alpha}^{BGK}(f_\alpha)$ ¹²
- Boltzmann collision integral: $C_{\alpha\beta}^B(f_\alpha, f_\beta, \Omega)$:

$$C_{\alpha\beta}^B = \int_{\mathbb{R}^N} dv_\beta \int_{S^{N-1}} d\Omega [f(v'_\alpha)f(v'_\beta) - f(v_\alpha)f(v_\beta)] K(|v_\alpha - v_\beta|, \Omega)$$

where $f : \mathbb{R}^N \mapsto \mathbb{R}_+$. This will be relevant for the case of charged particle - neutral interactions

- Weak form of a Landau collision operator $C_{\alpha\beta}^L$ ¹³

We will investigate IDC and determine means for improvement

¹²Manheimer, Wallace. et al. *The development of a Krook model for nonlocal transport in laser produced plasmas*. Physics of Plasmas **15**, 083103 (2008)

¹³Gamba, Irene. et al. *A conservative spectral method of the Boltzmann equation with anisotropic scattering and the grazing collisions limit*, arXiv:1306.4625



Electrostatic sheath physics

Upon completion of the above goals, we aim to simulate two charge species to explore **electrostatic sheath physics**.

- Bohm sheath theory applicable for collisional plasma
- Boundary work \Rightarrow can model *sheath*
- Accurate collisions \Rightarrow can model *presheath*
- kinetic solutions with self-consistent field calculations \Rightarrow *sheath edge (se)* kinetic Bohm criterion can be checked on ion density function f^i

$$\int_0^\infty \frac{f_{se}^i(v)dv}{v^2} \leq \frac{m_i}{kT_e}$$

Alternatively, our kinetic solutions will allow the above Bohm criterion to be used as a boundary condition so that simulations of only the edge are possible.



Higher dimensions

If possible, higher dimensions will be pursued

- ① an additional velocity dimension \Rightarrow magnetic fields and collisions can be included
- ② an additional spatial dimension \Rightarrow analysis of electrostatic effects in the edge and cross-field B transport

The above lends itself towards analyzing 2D edge problems and scrape-off layer transport.

Summary and conclusions



Conclusions

Motivations:

- **Goal**: simulating electrostatic plasma systems
- Eulerian schemes: CFL time restriction, high resolution mesh, large memory requirements
- Lagrangian schemes: no CFL restriction, propagator for a given problem required, phase space cells filament
- Semi-Lagrangian (SL) schemes: no CFL restriction, convect phase space fluid along known particle characteristics

The **convected scheme** (CS) is selected among SL methods:

- simple to implement (cf. discontinuous Galerkin)
- advection equation solutions can be made high order
- split operator methods disassemble higher dimensional equations into 1D advection equations in phase space \Rightarrow can use foundation of CS solvers for higher dimensions



Conclusions, cont'd

Summary:

- Two varieties of CS have been implemented, distinguished by how corrections (derivatives) are computed:
 - FDN methods – by finite differences (*FD5* shown)
 - FN methods – calculated in Fourier space (*F2 – F21* shown)
- 1D solvers applied to advection eqs.: $v = \text{const}$ and $v = v(x)$
- Time splitting algorithms were implemented:
 - LF2 – 2nd order, 1 stage
 - Y4 – 4th order, 3 stages
 - O6-4 – 6th order, optimized, 6 stages
 - O11-6 – 6th order, optimized, 11 stages
- These methods were demonstrated with test cases:
 - 2D rotating advection equation
 - 1D-1V Vlasov equation with prescribed \vec{E} -field



Conclusions and summary, cont'd

Conclusions and research proposals:

- Extend code to handle **1D-1V Vlasov-Poisson system** with self-consistent field calculations
- Inclusion of boundary \Rightarrow **Harten filter**
- Inclusion of collisions \Rightarrow **Deferred correction methods**
- With the above goals achieved \Rightarrow can simulate sheath physics
- If progress permits, we will work towards increasing the dimensions:
 - additional velocity dimension (1D-2V) \Rightarrow can include collisions and magnetic fields \Rightarrow **Boltzmann-Maxwell** system
 - additional space dimension (2D-2V) \Rightarrow analysis of cross-field interplay with edge transport \Rightarrow **scrape-off layer transport**, magnetic field \Rightarrow Bohm-Chodura criterion and **magnetic presheath** can be explored



Thanks!

Thank you!